1092

DECEMBER 1974 MATT-1092

EXPERIMENTS ON THE ADIABATIC TOROIDAL COMPRESSOR

BY

K. BOL, J. L. CECCHI,
C. C. DAUGHNEY, F. DEMARCO,
R. A. ELLIS, JR., H. P. EUBANK,
H. P. FURTH, H. HSUAN,
E. MAZZUCATO, AND R. R. SMITH

PLASMA PHYSICS LABORATORY

PRINCETON UNIVERSITY
PRINCETON, NEW JERSEY

This work was supported by U. S. Atomic Energy Commission Contract AT(11-1)-3073. Reproduction, translation, publication, use, and disposal, in whole or in part, by or for the United States Government is permitted.

DISCLAIMER

Experiments on the Adiabatic Toroidal Compressor*

K. Bol, J. L. Cecchi, C. C. Daughney, F. DeMarco,† R. A. Ellis, Jr.
H. P. Eubank, H. P. Furth, H. Hsuan
E. Mazzucato, and R. R. Smith

Plasma Physics Laboratory, Princeton University
Princeton, New Jersey 08540 USA

ABSTRACT

Magnetic compressional heating of a tokamak discharge has been demonstrated successfully in the Adiabatic Toroidal Compressor (ATC). In addition to these investigations of compressional heating, other basic measurements have been made on ATC recently. These measurements are of interest because the ATC incorporates an air-core transformer and dispenses with the usual copper shell, two features likely to be found on future larger devices with smaller aspect ratios. The following topics will be discussed: (1) characteristics of the uncompressed discharges in ATC, including the dependence of β_p on discharge parameters, bolometric measurements of the energy balance, measurements of the concentration of impurities; (2) MHD behavior and attempts at stabilization of the m = 2 kink-tearing mode.

I. INTRODUCTION

Magnetic compressional heating involving a large change in major radius has been successfully demonstrated in the Adiabatic Toroidal Compressor (ATC). A general discussion of slow adiabatic compression has been given by Furth and Yoshikawa[1] and the first experimental results obtained on ATC have been published.[2-4] Typical pre- and post-compression parameters are listed in Table I. Two of the distinctive features of ATC, the use of an air-core transformer and the absence of a conductive liner, are very likely to be found on future larger devices with smaller aspect ratio, so that the detailed investigation of the precompression plasma of ATC is of special interest. The design of ATC has also permitted the study of plasma heating by injection of high-powered neutral beams.[5,6]

In section II, the ATC device is described and compression results are summarized. In Section III, some characteristics of the uncompressed ATC discharges are considered including: the scaling of the poloidal beta, β_p, with discharge parameters; bolometric measurements of energy balance; and the concentration of impurities. In section IV, the MHD behavior and attempts to stabilize the kink-tearing mode are discussed.

II. THE ATC DEVICE

The major radius compression in ATC is produced by increasing the vertical equilibrium field, B_v , in a time which should be long compared with the particle collision time and short compared with the energy confinement times. For a plasma assumed to obey infinite-conductivity MHD theory, simple scaling laws have been derived[1] which give the plasma behavior for various modes of compression. The compression in ATC is carried out in a static toroidal field for which the following relations hold if $C = R_i/R_f$, where R_i is the initial major radius, and R_f is the compressed major radius and i and f denote the initial and compressed states, respectively, $T_f/T_i = C^{4/3}$; $n_f/n_i = C^2$; $a_f/a_i = C^{-1/2}$; and $I_f/I_i = C$ where T, n, a, and I denote temperature, density, minor radius, and plasma current exclusive of skin current.

The magnetic field configurations of the vertical equilibrium (and compression) field and of the ohmic transformer field are shown in Fig. 1 for the following states: just prior to the discharge; during the precompression phase; and during the compression. The physical arrangement of the poloidal field coils and a cross section of the vacuum vessel and of a toroidal field coil are shown in Fig. 2. The standard tokamak diagnostic systems are in routine use on ATC. The vacuum vessel is a stainless steel bellows without an insulating break. Originally four pumps with a pumping speed of $\approx$ 2000 liters/sec produced a base pressure of $2\text{-}4 \times 10^{-8}$ Torr after discharge cleaning with several thousand 2 msec 20 kA discharges in a mixture of hydrogen and neon. It has proved possible to obtain satisfactory discharges with only one pump although the base pressure increased as the number of pumps was reduced. The limiters for most of the discharges presented here were molybdenum top and bottom rails and inner and outer segments which conformed to the shape of the vacuum vessel. Only the inner limiter segments show significant erosion which occurs after compression and is attributed mainly to the effect of the high densities and thermal energies of compressed discharges which almost invariably terminate on the inner limiters. Recently it has been possible to use stainless steel limiters without any evidence of either excessive impurities in the discharge or damage to the limiters.

Figure 3 illustrates the operating cycle of ATC. After preionization by a 100 kHz oscillator, the transformer and vertical field windings are energized by the currents I_{OH} and I_v which respectively induce the plasma current and determine the major radius. The transformer field becomes large for $R < 60$ cm which requires that the transformer be current-biased so that I_{OH} is near zero at the time of compression, the precise value being an important compression parameter. The I_{OH} current waveform is determined by the discharge of capacitor banks and the I_v waveform up to compression is determined by an amplifier which also provides control of the major radius of the plasma current by a feedback loop involving an array of magnetic probes as position sensors. At a pre-determined time a capacitor bank is discharged into the B_v windings, rapidly increasing B_v and causing the compression. The compression field reaches a peak in about 2 msec and slowly decays. The compressed plasma equilibrium is governed by the decay of the currents in the B_v and OH windings, which are not controlled externally. The discharge in Fig. 3 slowly decreased in major radius until it terminated in a disruptive instability caused by contact with a limiter protecting the inner surface of the vacuum vessel.

Table I summarizes typical parameters for uncompressed and compressed discharges in ATC. The density and the ion temperature generally follow the expected behavior ($n \sim C^2 \approx 5$, $T_i \sim C^{4/3} \approx 3$) whereas the electron

temperature tends to be directly proportional to the compression ratio. Figure 4 shows that this difference in behavior also occurs for partial compressions. The difference presumably reflects the fact that the compression time τ_c is intermediate with respect to the ion and electron energy replacement times τ_i and τ_e, respectively: $\tau_i > \tau_c \sim \tau_e$.

The total plasma current should ideally be such that the poloidal flux linked by all of the plasma ring remains constant. Usually there is some decrease in this external flux during compression, so that the total current undergoes a somewhat smaller increase than would be expected in the ideal case.

TABLE I. Typical ATC Parameters

	Before Compression	After Compression
Major Radius R	90 cm	38 cm
Minor Radius a	17 cm	10 cm
Toroidal Field B_t	15 kG	46 kG
Plasma Current I_p	60 kA	150 kA
Ion Temperature T_i	200 eV	600 eV
Electron Temperature T_e	1 keV	2 keV
Average Electron Density $\bar{n}_e$	$1\text{-}2 \times 10^{13}$ cm^{-3}	10^{14} cm^{-3}

III. SOME CHARACTERISTICS OF THE ATC UNCOMPRESSED DISCHARGES

The time behavior of the loop voltage, plasma current, average density, and peak electron temperature of a typical ATC discharge are shown in Fig. 5. The electron density continues to increase long after the ionization of the filling gas, indicated by the break in the density curve shortly after the start of the discharge. This is an indication of a large influx of gas during the discharge which has been shown to be mainly hydrogen from the vicinity of the limiter. Figure 6 shows two temperature and density profiles which were taken (with Thomson scattering) during later portions of the discharges when a quasi-steady state has been reached. The electron temperature profile is always more narrow than the density profile and the average temperature is relatively independent of the density. For the profiles shown in Fig. 6, the toroidal field and plasma current were the same; the electron temperature profiles are almost identical although the densities differed by a factor of two.

The measured resistance of the plasma column is always 2 to 5 times larger than the value calculated from the temperature profiles assuming a $Z = 1$ plasma and neglecting trapped particle effects. Assuming that the increased plasma resistivity is due to an enhancement of the collision frequency which is independent of radius and affects trapped and untrapped particles alike, we found that trapped particle effects are unimportant.

The poloidal beta, $\beta_p \equiv 8\pi < nkT_e > / B_\theta(a)^2$, and the safety factor, $q(r)$, can be calculated from the Thomson scattering profiles. For the computation of q, the current density is assumed proportional to $T^{3/2}$. In Figs. 7 and 8 the results obtained in the following ranges of parameters are summarized: $12 < B < 20$ kG ; $0.8 < n_e < 2.5 \times 10^{13}$ cm^{-3} ; $500 < T_e\text{max} < 1500$ ev ; $50 < I_p < 100$ kA ; $85 < R < 90$ cm; and $a \approx 17$ cm. As shown in Fig. 7a, in which $\beta_p / < n_e >$ is plotted against $q(0)$ for nearly constant values of $q(a)$, $q(0)$ is seen to be a significant parameter because for $q(0) > 1$ the poloidal beta seems to be proportional to the density and for $q(0) < 1$, $\beta_p / < n_e >$ decreases almost linearly. Similar

behavior is exhibited in Fig. 7b in which data obtained with values of q(a) between 3.5 and 7.0 are included. These data yield a value of the ratio $\beta_p/< n_e >$ equal to 2.5×10^{14} cm^{-3} for $q(0) > 1$.

The electron energy confinement time, τ_E , defined as the ratio of the plasma electron energy to the Ohmic power input is proportional to the ratio of β_p to the resistance, Ω , of the column. Therefore, in our case τ_E is proportional to $< n_e >/\Omega$ if $q(0) > 1$ and is also directly proportional to $q(0)$ if $q(0) < 1$. This dependence of τ_E is shown in Fig. 8.

If it is assumed that the plasma resistivity has the classical dependence on T_e , then τ_E in ATC has a similar dependence on T_e and $< n_e >$ to that reported in Ref. 5. However, in ATC, τ_E is also inversely proportional to the resistivity enhancement factor and also decreases with $q(0)$ as $q(0)$ falls below one.

Gross properties of the energy balance in ATC have been investigated in terms of the energy loss to the limiter and through the plasma surface. The energy loss associated with charged particle diffusion and thermal conduction was monitored by measuring the temperature of the limiters. The radiation and the charge-exchange losses were detected by a bolometer devised out of a thick film flake thermistor, which had a time resolution of $\approx$ 1 msec. Peak plasma currents ranged from 40 kA to 90 kA . Some new findings are that (1) of the 60-80% of the total energy going to the limiters, the greatest part arrives during the steady state phase of a normal discharge. (2) At the termination of the discharge, the energy loss occurs mainly through the surface via radiation and/or charge-exchange. The amount of surface energy loss at the termination is larger than the stored plasma kinetic energy and is shown to include a large portion of the poloidal magnetic energy for a current larger than 50 kA . In addition to the above findings, our measurement has confirmed the results of other existing tokamaks.[6,7] These results are as follows: (1) The charged particle loss and the thermal conduction loss are the major mechanisms for the energy loss in our operating region of the discharge current. (2) Radiation loss constitutes less than 20% of the total energy loss before the current decays, with some evidence that the percentage rises with current. (3) Impurity contamination can greatly increase the radiation loss. This was demonstrated by injecting about 10% of neon into the hydrogen working gas, which almost doubled the radiation loss. (4) Disruptive instability also enhances the radiation loss. This was observed as the disruptive instability occurred but not in a controlled reproducible manner.

Measurements of the impurity concentration were carried out using a calibrated grazing-incidence monochromator looking horizontally along the major radius 135° away from the limiter in the midplane of the torus. The procedures of Hinnov and Hofmann[8] were used for calibration and evaluation of the data. The limits on impurity concentration obtained for typical discharges ($< n_e > \approx 2 \times 10^{13}$ cm^{-3}) are (all in cm^{-3}): $8 \times 10^{10} <$ Oxygen $< 4.5 \times 10^{11}$; Carbon $< 10^{10}$; Molybdenum $< 10^{10}$; $3 \times 10^{9} <$ Iron $< 1.5 \times 10^{10}$. Nitrogen was negligible except immediately after opening the vacuum system to air. The accuracy of the measurements is estimated to be ± 40% for oxygen and somewhat higher for iron and molybdenum. The concentrations of impurities given here are representative of tokamaks of this size. These values of impurities give values of $Z_{eff} = \Sigma\, n_i Z_i^2/n_i Z_i$ (where n_i is the concentration of the ions with charge Z_i) in the range $Z_{eff} \approx 2$-4 . The Z_{eff} determined from resistivity measurements is ~ 4-6 . The impurity data, together with some measurements of the absolute intensity of the hydrogen

light yield estimates of the particle confinement times which lie in the range 20-25 msec.

IV. MHD BEHAVIOR AND EXPERIMENTS WITH m = 2 MODE

1. MHD Behavior

Poloidal magnetic field perturbations have been observed on ATC and are qualitatively similar to those observed on other devices.[9,10] The slowly changing, oscillating kink-like modes have structures of the form

$$A_{mn} \exp[i(m\theta - n\phi - \omega_{mn} t)]$$

where θ and ϕ are the poloidal and toroidal angles, respectively, m and n are integers, and ω_{mn} is the angular frequency of the m , n mode. Perturbations with m = 2, 3, 4 and n = 1 have been observed with frequencies in the range 5 - 25 kHz , the m number being determined with an array of poloidal field pickup coils spaced 30° apart in the poloidal direction on the outer 180° of the ATC, and the n number with 4 coils spaced 90° apart in the toroidal direction.

The occurrence of the modes has been compared with tearing mode theory,[11] assuming the current density to be proportional to $T_e^{3/2}$, and choosing that one of the four current profiles given in Ref. 11 which best fits the data. In general, the theoretical prediction is that as the current is raised a mode may first appear when the rotational transform near the magnetic axis resonates with the mode; i.e., $2\pi/\iota = m$. When the resonant surface moves out to large enough radius, the mode becomes stable, the precise limit depending on the current profile, although for any profile the m = 2 is unstable out to larger radii than the m = 3 . Our findings are that the theory accommodates the m = 2 reasonably well, but that the m = 3 can still occur when the resonant surface is beyond the theoretical limit.[12]

2. Experiments With the m = 2 Mode

It is in general possible to pass rapidly through the current range in which modes with m > 2 are unstable, and it is presently unclear that these modes have much effect on plasma transport. The m = 2 mode, on the other hand, even when it does not lead to the disruptive instability[13,14] still has a deleterious effect on plasma confinement, and its stabilization or avoidance must be an important goal of tokamak research. Operation at currents above the unstable range may be a possibility[11,15] but it has received only brief attention on ATC. The other approach, stabilization of the mode, has been attempted with feedback and pulsed fields. These experiments are discussed below.

(a) Feedback experiments. Figure 9 shows one arrangement of control loops and magnetic pickup coils. The control loops generated a poloidal magnetic field having m = 2 , n = ±1 symmetry, and unavoidable higher harmonics. However, the results were insensitive to the details of control loop arrangement: essentially the same results were obtained using only the two outermost control loops, and again with two pairs of loops outside the vacuum vessel that subtended approximately 35° each in major azimuth. The pickup coils were located on the midplane and oriented to minimize their mutual inductance to the control loops; opposite coils were connected in pairs in order to cancel the main (n = 0) poloidal fields, as well as the m = 4 , n = 2 harmonic that may accompany the m = 2 . The signals from two such pairs 90° apart in major azimuth were added in suitable proportion to obtain a signal shifted by an arbitrary amount from a reference phase tied to the

mode. After going through a series of phase and amplitude compensation circuits, the signal was fed to a half megawatt amplifier, transformer-coupled to the control loops. The compensation was necessary because the lowest frequency pole in the equivalent circuit of the vacuum vessel lies at $f \cong 10$ kHz , within the range of frequencies spanned by the $m = 2$ mode. Amplifier phase shift from input signal to control current, after compensating, was 90^o at 22 kHz and 180^o at 55 kHz . The amplitude response was flat (3 db) to 32 kHz . The overall loop gain was only about 0.5 , at the limiter radius, and perhaps half that at the $q = 2$ surface. Within a factor of 2 this was the highest gain at which it was possible to operate: for small mode amplitudes the limit was set by the residual coupling between the control loops and the pickup coils, and for saturated modes by the maximum power of the amplifier.

For a linear system described by a dispersion equation with well separated poles, it is easy to see that with weak (low gain) feedback the perturbed poles execute circular paths about the original ones when the loop phase shift is varied from 0 to 2π , the radius of the circle being proportional to the gain.[16] This is roughly the effect that was observed, as shown in Fig. 10, although the mode was certainly not in the linear regime but, in fact, nearly saturated. Distortion of the signal made the amplitude variation difficult to evaluate, although the fundamental frequency was well defined; a Fourier analysis of the signal to evaluate the fundamental content would no doubt have improved the data.

Apart from the practical difficulty of attaining sufficient isolation between pickup coils and control loops it is clear that sensing the mode by the magnetic disturbance produced outside the plasma is in any case unsatisfactory. For it has been demonstrated experimentally,[17,18] in conformance with theoretical expectation,[11] that the mode is initially localized to the $q = 2$ resonance surface, and has then no detectable magnetic manifestation outside the plasma column. The mode may be harmless to the plasma in its earliest stages but amplifier economy certainly demands that it be kept to the lowest possible level. It should be possible to develop the x-ray technique described in Ref. 19 and elsewhere[18,20] to meet the need, provided present results continue to hold at higher loop gain, i.e., that maximum stabilization of the mode will occur with a loop phase shift for which the frequency shift is not too large.

(b) Mode-locking. To obtain the mode-locking results the feedback loop was opened and the amplifier driven from a signal generator. In general, a control field at the plasma surface of about half the mode amplitude secures locking; however, the threshold is not sharply defined: the mode may jump in and out of synchronism before locking to the control signal, and is locked more easily when saturated than when still growing.

Whereas the threshold shows little frequency dependence, Fig. 11 shows the phase between mode and control signal to vary markedly with frequency. The phases have been corrected for the vacuum vessel, and in addition the phase of the pickup coils located near the control field nodes has been shifted by 90^o to make it correspond to the coils near the antinodes. Thus the divergence of the points at low frequencies implies that the locked mode is no longer a single rotating wave; a difference in amplitudes observed at the two locations shows that a standing wave component is generated which becomes dominant at frequencies below $\sim 0.2\, f_{mode}$, the larger amplitude occurring at the control field antinodes. (Note that the pickup coils should not couple to the equilibrium distortions of the magnetic surfaces produced by the control fields.)

It is interesting that when mode-locking occurs, it apparently takes place throughout the plasma within a fraction of a cycle, according to the signals obtained from the pickup coils and from x-ray detectors monitoring emission from the plasma core.[20] Presumably, then, the effect propagates through the plasma on the hydromagnetic time scale; skin penetration times would be orders of magnitude longer. The implication of this result would seem to be that the saturated m = 2 oscillations do indeed result from a rotating quasistable helical equilibrium,[21] and that the shear free rotation around the minor axis is due to an appropriately varying radial electric field which compensates for the variation of the electron diamagnetic drift frequency with radius.

Finally, the relative ease with which mode-locking occurs also suggests that when two modes are present simultaneously--as an m = 1 and 2 , or an m = 2 and 3--they might lock together as soon as one of the pair has reached large enough amplitude. Such synchronism between the m = 2 and 3 has been observed on the ST Tokamak, where the m = 2 was detected by means of x-ray emission and the m = 3 by magnetic pickups.[22]

(c) Mode-locking and stabilization by pulsed fields. The most usual result of passing a current pulse of sufficient strength through control loops generating an m = 2 , n = 1 magnetic field component is mode-locking at zero frequency. This is shown by Fig. 12, where the mode amplitude is still small when rotation is stopped, but where the mode appears fully saturated when rotation is resumed. The phase of the stationary mode with respect to the applied field is difficult to determine precisely, because transient perturbations accompany and obscure the locking phenomenon. In general, it appears that the field of the locked mode may lag the control field by any phase angle from 180° - 360° . It is not clear how this result should be related to the measurements shown in Fig. 11. It may be noted that the pulsed experiments were done with the external loops because the internal ones could not withstand the electromechanical forces.

Discharges tend to be unfavorably affected when mode rotation is suppressed: in high current discharges which are limited by the disruptive instability, onset of the disruption occurs earlier, on the average, when rotation is suppressed; when the control field is raised above the level needed to stop rotation, small-scale disruptions (Fig. 13) occur with increasing frequency. Furthermore, plasma density, which ordinarily rises more slowly--if at all--when an m = 2 kink is present than when it is not, frequently dropped by ~ 10% during the 5-10 msec that rotation was suppressed in typical cases.

Under certain conditions it appears that the mode can indeed be stabilized by the control field. Thus, Fig. 14 shows a case in which the rotation persists, but the amplitude slowly decreases to the noise level over some tens of cycles. We believe that one of the preconditions for this effect is that the mode is not too violently unstable, but a more precise prescription cannot yet be given.

REFERENCES

* Supported by USAEC Contract AT(11-1)-3073.

† Present address: Laboratori Gas Ionizzati, Frascati (Italy).

[1] FURTH, H. P., YOSHIKAWA, S., Phys. Fluids 13, 2593(1970).

[2] BOL, K., et al., Phys. Rev. Letters 29, 1495(1972).

[3] BOL, K., et al., Proceedings of The Third International Symposium on Toroidal Plasma Confinement (Garching bei MÜnchen, 1973), Max Planck Institut fÜr Plasma Physik, Paper B-12.

[4] ELLIS, R. A., et al., Proceedings of The Sixth European Conference on Controlled Fusion and Plasma Physics (Moscow, Joint Institute for Nuclear Research, 1973), Vol. 1.

[5] ARTSIMOVICH, L., et al., Plasma Physics and Controlled Nuclear Fusion Research (International Atomic Energy Agency, Vienna 1969), Vol. I, p. 157.

[6] GORELIK, L. L., MIRNOV, S. V., NIKOLAEVSKY, R. G., SINITSYN, V. V., Nucl. Fusion 12, 185(1972).

[7] DIMOCK, D. L., EUBANK, H. P., HINNOV, E., JOHNSON, L. C., MESERVEY, E. B., Nucl. Fusion 13, 271(1973).

[8] HINNOV, E., HOFMAN, F. W., Journal Optical Society of America 53, 1259(1963).

[9] MIRNOV, S. V., SEMENOV, I. B., At. Energ. 30, 14(1971) [Sov. At. Energy 30, 14(1971)].

[10] HOSEA, J. C., et al., in Plasma Physics and Controlled Nuclear Fusion Research (IAEA, Vienna, 1971) II, p. 425.

[11] FURTH, H. P., RUTHERFORD, P. H., SELBERG, H., Phys. Fluids 16, 1054 (1973).

[12] We are indebted to S. VON GOELER for alerting us to the possibility on the basis of similar observations on the ST Tokamak.

[13] BOWERS, D. L., et al., Plasma Physics 13, 849(1971).

[14] ARTSIMOVICH, L. A., Nucl. Fusion 2, 215(1972).

[15] VLASENKOV, V. S., et al., Garching, München Conference (1973) paper B2.

[16] THOMASSEN, K. I., Private communcation.

[17] JOBES, F. C., HOSEA, J. C., Garching, München Conference (1973) paper B14.

[18] VON GOELER, S., Invited paper, APS Plasma Physics Conference, Albuquerque (1974).

[19] VON GOELER, S., STODIEK, W., SAUTHOFF, N., Phys. Rev. Lett. (to be published).

[20] SMITH, R. R., APS, Physics Conference, Albuquerque (1974).

[21] RUTHERFORD, P. H., FURTH, H. P., ROSENBLUTH, M. N., Fourth Conference on Plasma Physics and Controlled Thermonuclear Research, Madison, Wisconsin, 1971, Paper CN-28/F-16.

[22] VON GOELER, S., Private communication.

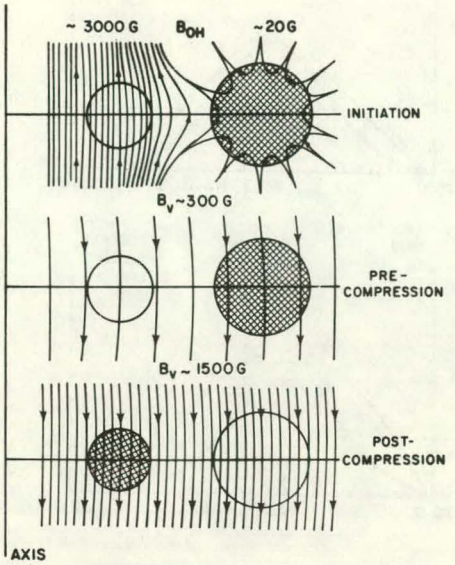

Fig. 1. Vertical equilibrium and Ohmic transformer field patterns.

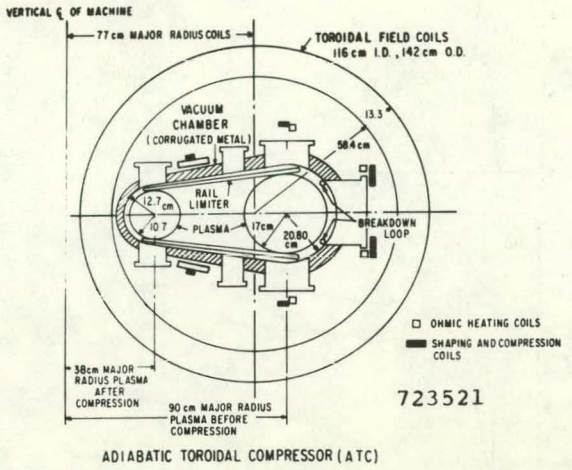

Fig. 2. Cross-section of ATC.

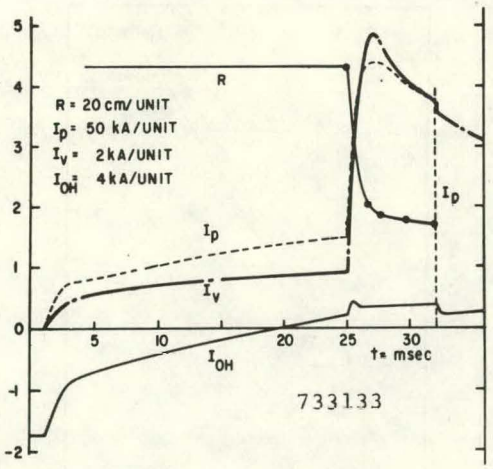

Fig. 3. Time variation of major radius, plasma current, vertical field current, and Ohmic transformer current during a compression discharge.

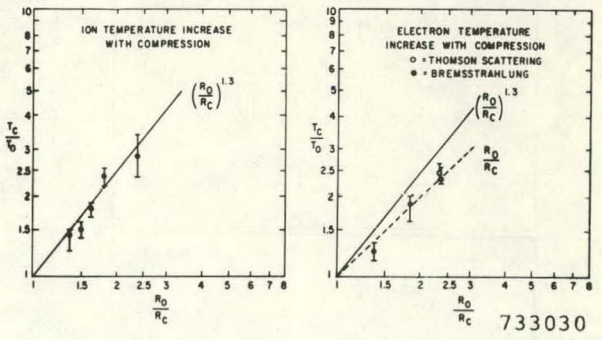

Fig. 4. Observed scaling of electron and ion temperatures.

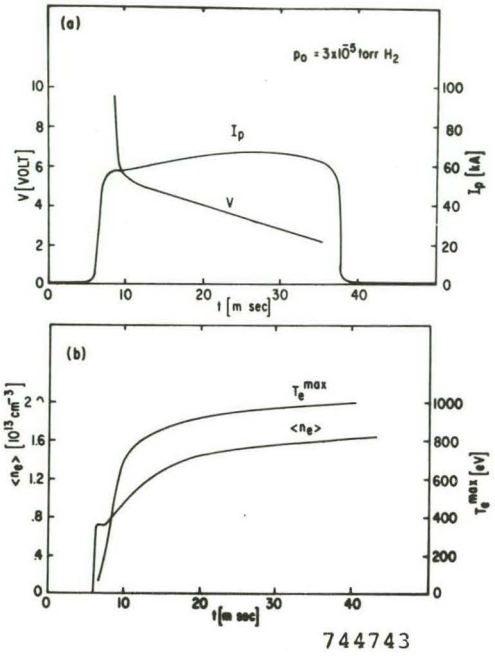

Fig. 5. Typical time behavior of plasma current, I_p; loop voltage, V; average electron density $\langle n_e \rangle$; and peak electron temperature, T_e^{max}.

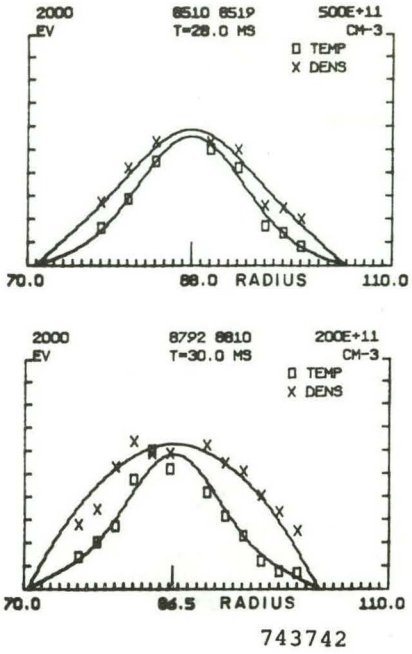

Fig. 6. Radial profiles of electron density and temperature. The plasma current (60 kA), the loop voltage, (3V), and the toroidal magnetic field (16 kG) were the same in both.

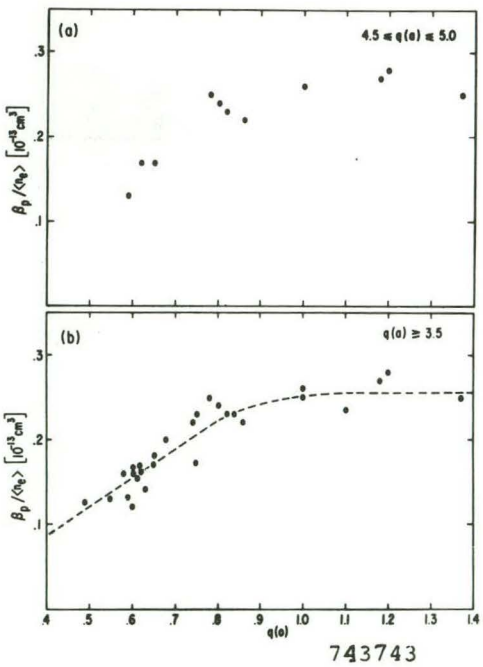

Fig. 7. Dependence of the ratio of the poloidal beta to the average electron density ($\beta_p/\langle n_e \rangle$) to the safety factor, q(0). The safety factor at the limiter was kept almost constant in (a) and varied from 3.5 to 7 in (b).

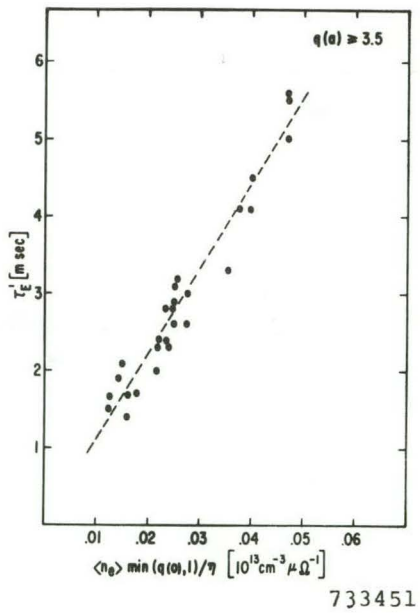

Fig. 8. Dependence of the electron energy confinement time, τ_E, on the average electron density, $\langle n_e \rangle$, the resistance of the plasma column, and the safety factor at the axis. Min[q(0),1] is the smaller of q(0) or 1.

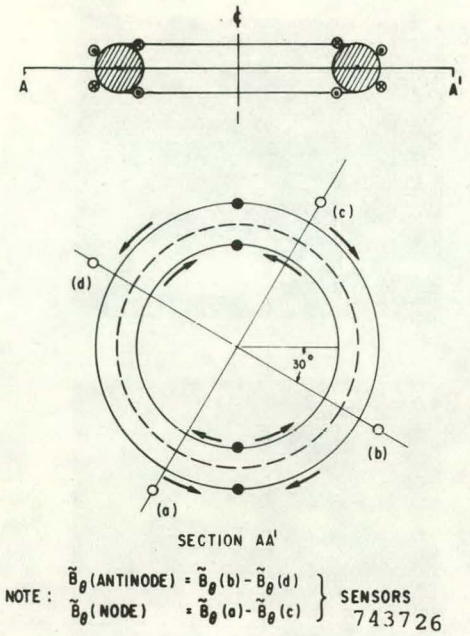

Fig. 9. Diagram of control loops and mode sensors.

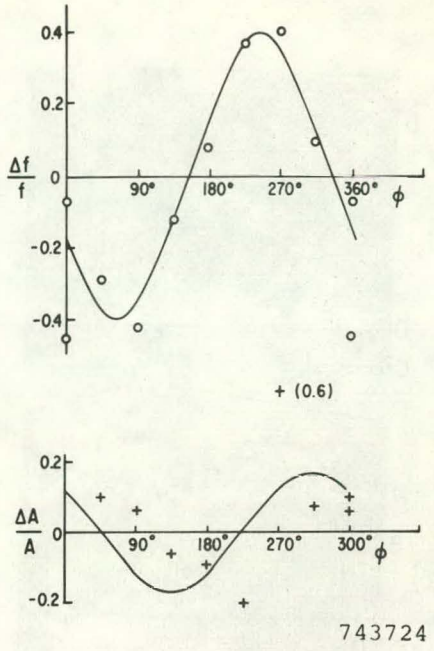

Fig. 10. Mode frequency and amplitude changes as function of feedback loop phase shift. Curves are least square fit of sinusoids to data.

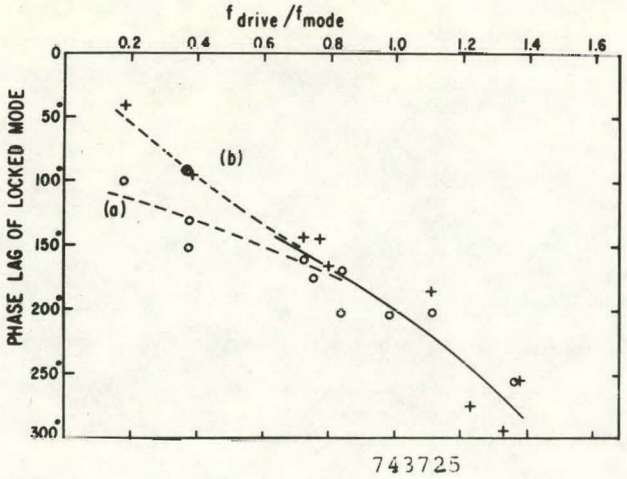

Fig. 11. Phase difference between locked mode and control field vs control frequency. (a) Phase at anti-node; (b) Phase at node +90°.

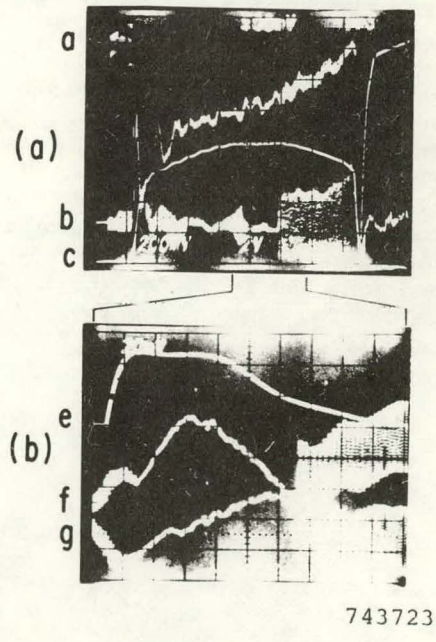

Fig. 12. Suppression of mode rotation by control pulse.
12-a: (a) Plasma voltage, -2V/cm; (b) Magnetic pickup signal (unintegrated); (c) Plasma current, 20 kA/cm.
12-b: (e) Control loop current, 200 A/cm; (f) and (g) integrated magnetic pickup signals from control field anti-node and node positions respectively.

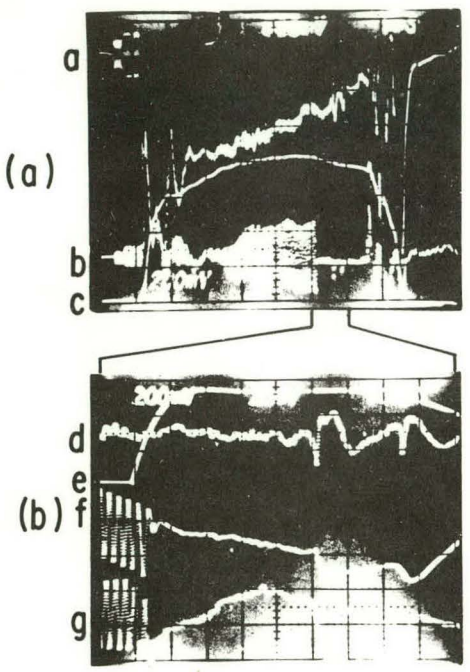

743722

Fig. 13. Detail of rotation arrest and mini-disruptions.
13-a: (a), (b), and (c) Plasma voltage, pickup signal, and plasma current respectively.
13-b: (d) Plasma voltage, 1 V/cm; (e) control loop current, 200 A/cm; (f) and (g) integrated pickup signals from control field node and anti-node positions, respectively. Arrows show when mode was in phase with control field. Two mini-disruptions occur in the quiescent interval.

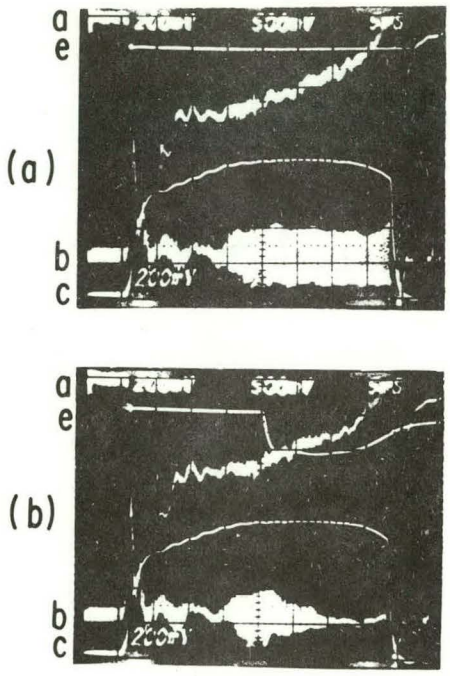

743721

Fig. 14. Mode stabilization by control pulse.
14-a: Zero control field (e).
14-b: With control field, 200 A/cm.